ASIA-PACIFIC JOURNAL OF CHEMICAL ENGINEERING
Asia-Pac. J. Chem. Eng. 2014; **9**: 134–145
Published online 1 July 2013 in Wiley Online Library
(wileyonlinelibrary.com) DOI: 10.1002/apj.1753

Research article

Operating windows of stripe coating

Chi-Feng Lin,[1] *Bo-Kai Wang,*[1] *Shao-Hsuan Lo,*[1] *David Shan-Hill Wong,*[1] *Ta-Jo Liu*[1]* *and Carlos Tiu*[2]

[1]*Department of Chemical Engineering, National Tsing Hua University, Hsin Chu, Taiwan 300*
[2]*Department of Chemical Engineering, Mohash University, Ciayton, Victoria, Australia*

Received 18 December 2012; Revised 21 May 2013; Accepted 26 May 2013

ABSTRACT: The fluid mechanics of narrow stripe coating for low viscosity Newtonian solutions was investigated. A narrow stripe could be produced either through a slot die with a shim to control the slot width or through a rectangular nozzle. A flow visualization technique was employed to observe the mechanism on how a narrow stripe breaks at high coating speeds. Two-dimensional and three-dimensional numerical simulations on coating flows were also carried out to examine the fluid motion. The coating solution was found to expand laterally after emanating from the slot die channel at low coating speeds. The stripe width contracts gradually with increasing coating speed until coating failures appear. The coating defect observed switches from ribbing to a periodic stable and break-up motion. The effects of various fluid properties, geometric and operating parameters on the variation of coating width and maximum coating speeds were examined. A universal correlation involving two dimensionless groups, Reynolds and Bond number, was established for the prediction of coating width. © 2013 Curtin University of Technology and John Wiley & Sons, Ltd.

KEYWORDS: narrow stripe coating; low viscosity Newtonian fluids; Reynolds number; Bond number; flow visualization; numerical solution

INTRODUCTION

Coating a narrow stripe has many industrial applications, such as installing a stripe adhesive or magnetic material on an identification card. Recently, several potential applications including the manufacture of radio-frequency identification device and color filters for LCD panels have emerged. The conventional method to produce color filters is to coat a RGB (red, green, and blue) solution on a large piece of glass, and through a series of etching and cleaning steps, RGB dots or stripes are created. Usually over 90% of the coating solutions are wasted.[1] A new and better approach is to coat narrow RGB stripes directly on a large piece of glass, whereby most of the RGB solution is preserved.[2] A recent survey on drying of stripe color filter materials reveals that coffee rings could form under certain drying conditions.[3] Hence, a thorough understanding of the coating mechanism of narrow stripes is required before this new approach can be accepted as a reliable production means.

Traditionally, a narrow stripe can be coated on a substrate by using a nozzle to deposit the coating solution. However, nozzles are difficult to assemble if simultaneous coating of multiple stripes is needed. Another approach is to insert a specially designed shim into a slot die to produce multiple stripes as discussed by Wen and Liu.[4] Because the coating width of the stripe is much smaller than the one produced from the conventional slot die coating, the edge effect is more critical on the product quality of the coated narrow stripe.

Slot die coating technology was invented by Beguin[5] in the early 1950s. Ruschak[6] first examined this coating method theoretically and proposed the concept of the stable operating window. Later, Higgins and Scriven[7] modified the theoretical solution of Ruschak by including the viscous effect. Lee *et al.*[8] determined the minimum wet thickness of slot die coating experimentally and found that there existed a critical capillary number. The minimum wet thickness was found to increase until it reaches the critical capillary number and then to become constant beyond that. By contrast, Carvalho *et al.*[9] showed , in their numerical solution, that the minimum wet thickness could decrease at high capillary number. More recently, Chang *et al.*[10] found experimentally that depending on the Reynolds number, the minimum wet thickness could either increase or decrease. The same research group[11–13] also examined the mechanism of start-up in slot die coating, the difference between slot die coating at horizontal or vertically downward position, and the effect of bead vacuum on slot die coating.

**Correspondence to:* Ta-Jo Liu, Department of Chemical Engineering, National Tsing Hua University, Hsin Chu, Taiwan 300. E-mail: tjliu@che.nthu.edu.tw

Several researchers have examined the motion of a liquid drop or stripe on a substrate. Dobroth and Erwin[14] studied the surface profile of a stripe. Huppert[15] considered the expansion of a viscous drop, and Vafaei and Podowski[16] studied the effect of gravity and surface tension on the expansion of a coated drop.[17] There were also several patents that described the delivery of multiple stripes with different die design approaches.[18,19]

In this study, the fluid mechanics of a single coated stripe, focusing on the coating width and the maximum coating speed, was investigated. The performance of a single narrow stripe produced by a single rectangular nozzle and one inserted with a specially designed shim into a slot die was compared. Two-dimensional and three- dimensional numerical simulations of the fluid motion of a single narrow stripe were also carried out.

EXPERIMENTAL

We limited our study on the width for a narrow stripe coating to be less than 4×10^{-4} m, so that edge effects could be significant and should be taken into consideration. Two different designs were used to generate a narrow stripe in the flow experiment. The first design was to insert a specially-constructed shim into an experimental slot die. The coating width could be adjusted by using different sizes of shim in the slot die. The other design was a simple rectangular nozzle used to deliver the coating solution. The geometry of the slot die is displayed in Fig. 1, with its geometric dimensions given in Table 1. Two die elements A and C, together with a shim B of thickness S were assembled together to deliver the coating solution. There were two straight semi-circular cavities with radii r_1 and r_2 inside the slot die to allow for the expansion of the coating solution to form a uniform liquid sheet when emanating from the die. To control the width of the narrow coated stripe, shims with different widths W, as shown in Fig. 1(b), were made. The coating widths were varied from 0.1 to 0.001 m. A photograph of the stainless steel rectangular nozzle as shown in Fig. 2(a) was used for the delivery of a narrow stripe. The cross sections of the steel bar, having a dimension of 0.0025 m × 0.0004 m, and the location of the rectangular opening, having a dimension of 0.001 m × 0.0001 m, are depicted in Fig. 2 (b). The major difference between the slot die with a shim and that with the nozzle is the lateral expansion of the coating solution. The expansion is boundless in the former geometry, whereas it is restricted in the latter case.

Dilute poly(vinyl) alcohol solutions were used as tested fluids. The chemical was supplied by Chang-Chun Petrochemical Co. (BP 24, Taipei, Taiwan). It has a molecular weight of approximately 120 000, and a degree of hydrolysis of around 86–89%. The concentrations of the poly(vinyl) alcohol solutions were low enough to ensure apparent Newtonian

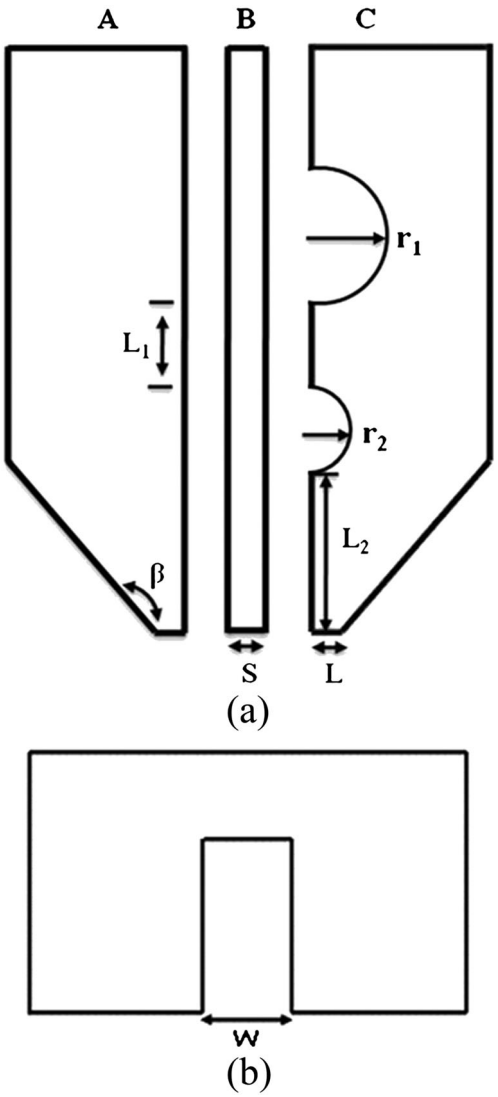

Figure 1. Geometry of (a) the laboratory slot die and (b) a shim.

Table 1. Dimensions of the slot die.

Geometric parameters of the die	Dimensions(m)
Slot gap (S)	0.0001, 0.0002
Length of the first flow channel (L_1)	0.008
Length of the second flow channel (L_2)	0.02
Radius of the inner manifold (r_1)	0.01
Radius of the second manifold (r_2)	0.003
Lip length (L)	0.0002
Coating gap (H)	0.0001, 0.0002, 0.0005
Angle at the die edge (β)	135°
Width of the flow channel (W)	0.001, 0.01, 0.1

DOI: 10.1002/apj

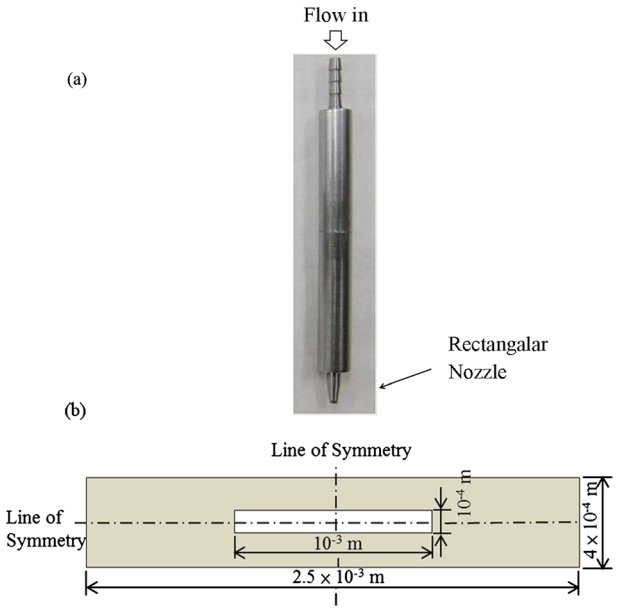

Figure 2. (a) Photo of the rectangular nozzle. (b) Dimensions of the nozzle opening (bottom view). This figure is available in colour online at www.apjChemEng.com.

behavior with relatively low viscosities. This property is essential for industrial applications of coating stripe. The fluid viscosity and surface tension were measured by Brookfield rheometer, (DV-III, Brookfield Engineering Laboratories, INC., Massachusetts, U.S.A) a surface tension meter (CBVP-A3, Kyowa Kaimukagako Co., Japan), respectively. The relevant physical properties of all test solutions are given in Table 2.

A small laboratory-scaled coater was used for the stripe coating experiments. Fig. 3(a) displays the schematic of the experimental setup. The coating solution was delivered into the slot die (A) after passing through a filter (F). The liquid film emanated from the slot die was coated onto a moving chrome-plated steel roller (B). The coated solution was removed by two squeegees (C) and then recycled. The flow experiment started at a low coating speed, dripping or leaking would appear, but as the coating speed increased these defects would disappear. The current experimental setup allowed for continuous experimental observation by flow visualization. The

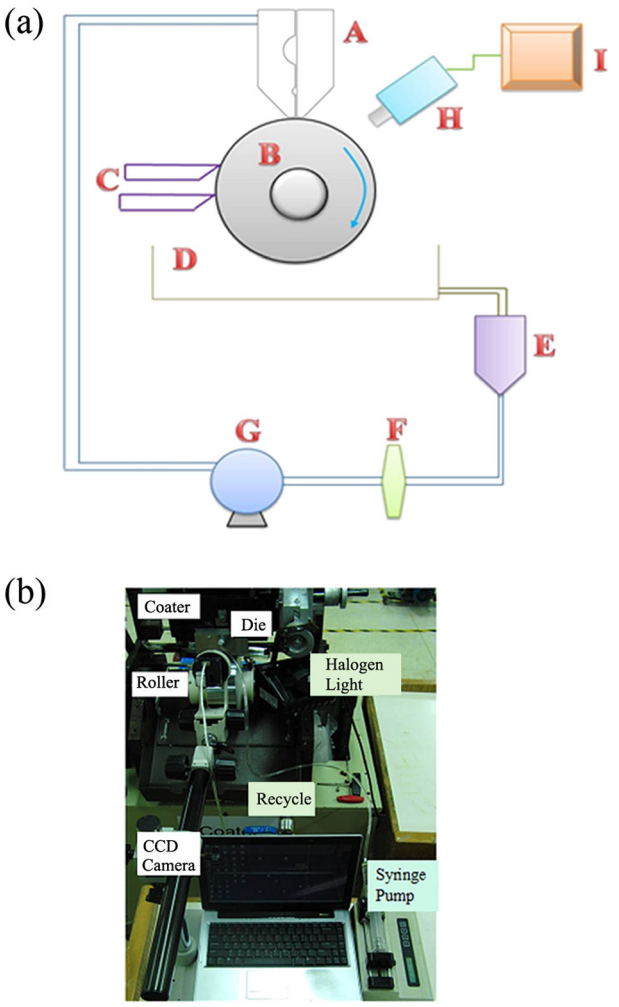

Figure 3. (a) Stripe coating experimental setup. (b) Photo of the flow visualization setup. This figure is available in colour online at www.apjChemEng.com.

same experiment setup was used for both shim-inserted slot die and rectangular nozzle coatings. The results obtained from these two different experiments were analyzed and compared.

To observe the fluid motion of stripe coating, a flow visualization technique was employed. A photograph of the flow visualization setup is shown in Fig. 3(b). A video camera (CP-4500, Nikon) was positioned at the top of the coater to observe the forming of stripe

Table 2. Physical properties of test solutions.

Type of solutions	Number	Viscosity (mPa s)	Surface tension (mN/m)	Static contact angle on the substrate (°)
PVA solutions	1	6.5	42.5	63
	2	6.5	28.5 (FSO added)	47
	3	6.5	21.5 (FSO added)	42
	4	10	22.0 (FSO added)	40
	5	24	21.1 (FSO added)	42
	6	45	20.2 (FSO added)	41

PVA, poly(vinyl) alcohol.
※FSO is a non-ionic surfactant produced by DuPont to reduce surface tension.

DOI: 10.1002/apj

on the substrate and the stripe width variation. The image taken could be magnified 24 times, and the minimum scale for identification was 3.0×10^{-4} m. Another microscope (SZ-6045, Olympus) with a magnifying power 64 was positioned to observe the coating bead from the side. The microscope was connected to a charge-coupled device camera (EX-F1, Casio) to record the images. The charge-coupled device camera was capable of taking pictures at 300 frames per second. Proper lighting was critical to catch the sharp images of both the upstream and downstream menisci. The focusing plane was positioned in such a way that the light was able to penetrate into the coating bead. Images were subsequently modified using software such as Photoshop or AutoCAD for better presentation.

Numerical simulation

A commercial software package FLOW-3D was utilized to simulate the narrow stripe coating flow. The flow geometry of the coating bead is displayed in Fig. 4. The figure depicts the coating fluid emanating from the slot exit and depositing on a moving web. The coating bead is bound by the upstream and downstream menisci, die lip, and the web, as colored in green on the figure. The mathematical formulation of the flow problem is given later on.

Consider an isothermal, steady and incompressible Newtonian fluid motion in the coating bead region. The dimensionless governing equations are as follows:

$$\nabla\cdot v = 0 \tag{1}$$

Eq. (1) indicates that the fluid is incompressible.

$$Re(v\cdot\nabla v) = \nabla\cdot T + St\mathrm{k} \tag{2}$$

Eq. (2) presents the dimensionless form of the equation of motion, the stress tensor T is defined as.

$$T = -p\mathrm{I} + \left[\nabla v + (\nabla v)^{\mathrm{T}}\right] \tag{3}$$

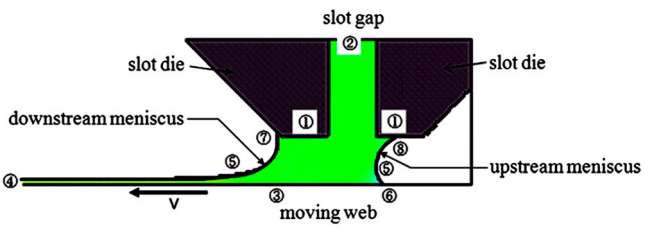

Figure 4. Flow geometry of the coating bead. ①: die wall surface, ②: inflow in the slot, ③: moving web, ④: outflow condition, ⑤: upstream and downstream menisci, ⑥: dynamic contact line, ⑦ and ⑧: static contact lines. This figure is available in colour online at www.apjChemEng.com.

The Reynolds number Re and Stokes number St are defined as

$\mathrm{Re}\equiv\rho q/\mu, \mathrm{St}\equiv\rho g H^2/\mu V$, respectively.

The corresponding boundary conditions as marked by numbers in Fig. 4 are as follows:

- Die wall surface ①: $v=0$ (4)
- Inflow in the slot ②: $v=\mathrm{u}$ (5)
- Moving web ③: $v=\mathrm{V}$ (6)
- Outflow condition ④: $\mathrm{n}\cdot\nabla v=0$ (7)
- Upstream and downstream menisci, two free surfaces ⑤:

$$\mathrm{n}\cdot T = \frac{1}{Ca}\mathrm{n}\nabla\cdot\mathrm{n} - \mathrm{n}P \tag{8a}$$

$$\mathrm{n}\cdot v = 0 \tag{8b}$$

Here, n is the unit vector normal to the free surface, Ca is the capillary number defined as $Ca\equiv\mu V/\sigma$, and $P\equiv P_{\mathrm{atm}}/\rho v$.

- Dynamic contact line ⑥:

$$\mathrm{n}\cdot T = \frac{1}{Ca}\mathrm{n}\nabla\cdot\mathrm{n} - \mathrm{n}P \tag{9a}$$

$$v=V \tag{9b}$$

- Static contact lines ⑦ :

$$\mathrm{n}\cdot T = \frac{1}{Ca}\mathrm{n}\nabla\cdot\mathrm{n} - \mathrm{n}P \tag{10a}$$

$$v = 0 \tag{10b}$$

The system was solved by the commercial software package FLOW-3D® by using the finite volume method. The downstream length was assumed to be long enough to ensure the rectilinear flow on the moving web.

The most critical part for solving the flow system was the determination of the upstream and downstream menisci accurately. A volume-of-fluid method was applied (Hirt *et al.*[20,21]) for the identification of the free surface positions.

Three groups of parameters were required as the input data for the numerical simulation. Group 1 included the physical properties of the coating solution such as viscosity, surface tension, density and the static contact angles of fluid on the slot die and on the web. Values of static contact angles had to be evaluated from the experiment or from existing data. Group 2 involved the geometric parameters such as slot gap, coating gap, die lip shape, and length. Group 3 consisted of the operating parameters such as flow rate and web speed. The shapes of the upstream and downstream menisci, the internal velocity, and the pressure field were generated by the numerical package FLOW-3D®.

DOI: 10.1002/apj

Square and cubic elements with 10 μm length on each side were used for 2D and 3D simulation, usually there were over 20 000 elements in one mesh. Details of the 2D and 3D simulations of coating flows were discussed by Lin,[22] and information on the commercial package FLOW-3D® could be found elsewhere (http://www.flow3d.com).

RESULTS AND DISCUSSION

The effect of channel width W on the coating stripe width was first examined using three different channel or shim widths in the slot die. Figure 5 shows the plot of Δw, the difference between the coating width, and the slot channel width, as a function of the coating speed *V*. As seen in the figure, Δw was large at low coating speed for all three channel widths, indicating a large degree of lateral spread of coating solution, and approached a constant value with increasing *V*. When the coating speed was increased beyond a critical value V_{max}, coating defects occurred. This critical speed was found to be a function of channel width, and it was much lower for the two wider channel widths than the one for the smallest channel, as identified by V_{max1} and V_{max2} respectively in Fig. 5. The coating defects observed at the two maximum coating velocities were substantially different. At V_{max1}, the coating defect was *ribbing*, similar to that observed in slot die coating of low viscosity solutions reported in previous studies.[8,10,12] This was expected as the two wider channel widths were closer to those reported previously in slot die coating. For the smallest channel width, a narrow coated stripe was observed to form, break and reform intermittently when the coating speed was increased beyond V_{max2}. This yielded a series of broken long coated stripes on the substrate. The mechanism of this repeated coat-and-break phenomenon was further investigated using several shim widths. The coating behavior was found to be similar to the generally observed slot-die coating flow if the shim width was above 5×10^{-4} m. Uniform coating surface could be maintained until the coating speed reached its maximum value at which the onset of ribbing occurred. However, the coating defect observed was different from the conventional slot flow if the shim width was below 5×10^{-4} m. There was no evidence of ribbing defect, instead a periodic breakup of the coated stripe was observed. Figure 6(a) and (b) show a sequence of photographs of coated stripes taken at increasing coating speed for shim widths of 2 and 4×10^{-4} m, respectively. At the initial onset of coating defect, the coating would break into 2 ~ 3 stripes and as the coating speed increased, the stripes would break for a short time and then start to coat again. The coat and break process was observed to be periodic. The frequency of coat and break increased and the length of stripe became shorter with increasing coating speed. The phenomenon was similar for these two shim widths, as seen in Fig. 6(a) and (b). Hence, the width between 2 and 4×10^{-4} m was considered as a transition region. If the shim width was decreased to around 1×10^{-4}m or smaller, the coated stripe would break periodically at a much higher coating speed. Because the coating behavior and its maximum coating speed observed in narrow channel, $w = 1.0 \times 10^{-3}$ m, were different from those of wider channel widths, the experimental results reported in the following figures were all based on this narrow channel.

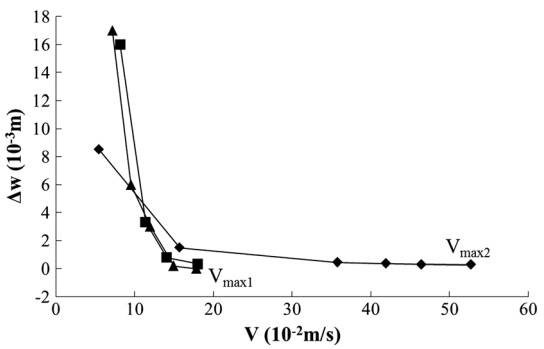

Figure 5. The effect of slot channel width *W* on the variations of coating width. ΔW = w-W, $\mu = 6.5$ mPa s, $\sigma = 42.5$ mN/m, $H = 1.0 \times 10^{-4}$ m, $L = 2 \times 10^{-4}$ m, $S = 1.0 \times 10^{-4}$ m, $Q = 4.67 \times 10^{-6}$ kg/s; ◆:$W = 1.0 \times 10^{-3}$ m; ■:$W = 1.0 \times 10^{-2}$ m; ▲:$W = 0.1$ m.

The effects of flow rate on the coating width and the maximum coating velocity are displayed in Fig. 7. Fig. 7(a) and (b) present the results obtained on the slot die with a shim width of 1×10^{-4}m and on the rectangular nozzle, respectively. As the flow rate increased, the spreading of the coating fluid appeared to be more significant and the maximum coating velocity was also extended. However, the stripe width continued to contract with increasing coating velocity and broke eventually when the coating width was reduced to approximately 20–30% of the of the slot channel width W. Comparing the two geometries, the coated stripe from the rectangular nozzle had less spreading at low coating speeds and could be operated at a higher maximum coating speed before the breakage of stripe. The coating solution could fill and expand laterally between the slot die and the moving roller, this lateral expansion could cause a wider stripe for the coating solution emanating from the slot die exit. The spreading was much wider than that of a rectangular nozzle because there was no support for lateral expansion in the rectangular nozzle. The coated stripe produced from a rectangular nozzle was deemed to be more stable because sharp contraction of the coated stripe could be avoided.

The effect of solution viscosity on stripe width obtained in both geometries is presented in Fig. 8(a) and (b). In slot die coating (Fig. 8(a)), higher viscosity

DOI: 10.1002/apj

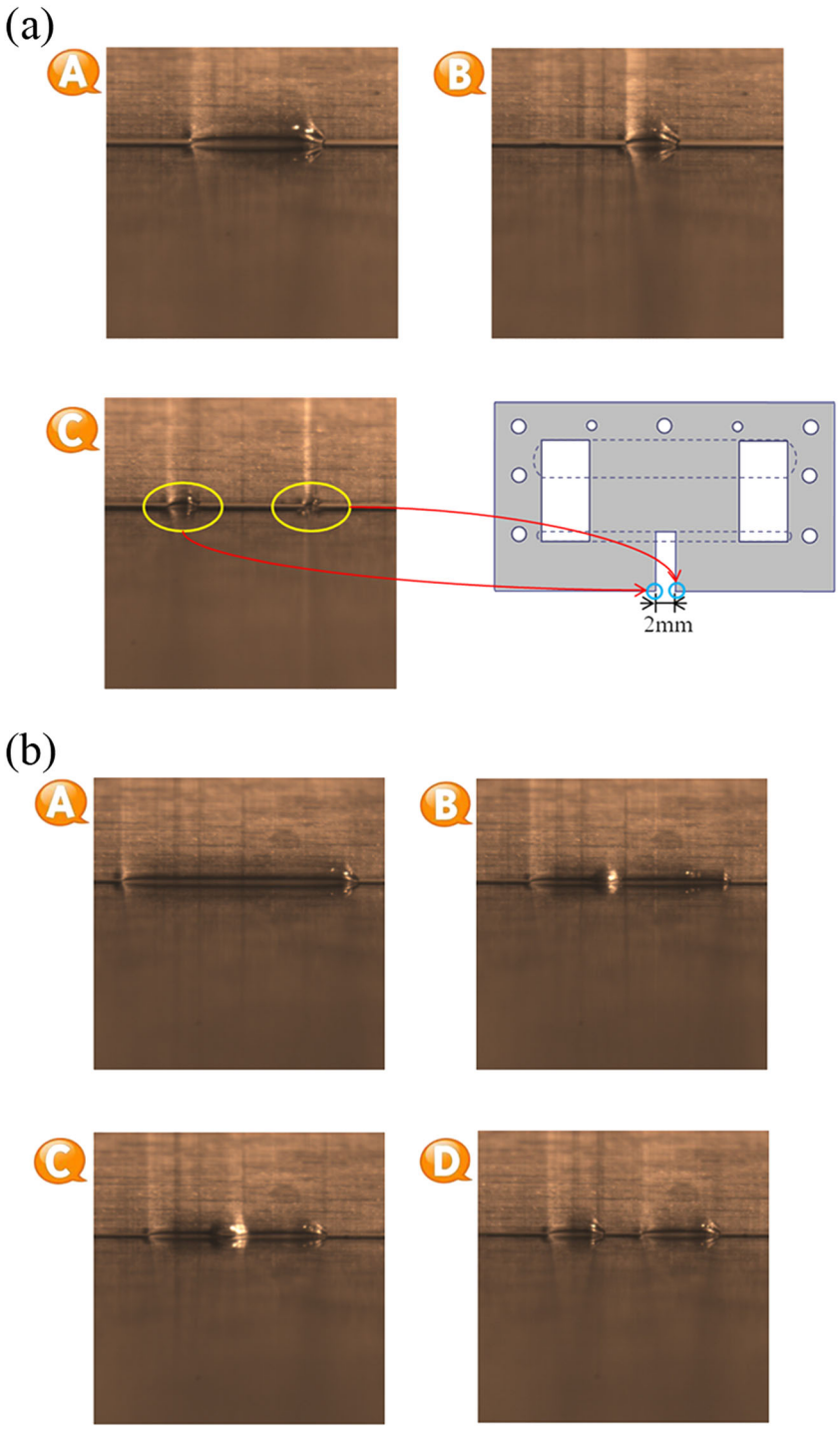

Figure 6. (a) Coating flow from a slot die with shim width 2×10^{-3} m, $u = 0.0464$ m/s; (A) $V = 0.160$ m/s; (B) $V = 0.323$ m/s; (C) $V = 0.540$ m/s; (b) coating flow from a slot die with shim width 4×10^{-3} m, $u = 0.0464$ m/s; (A) $V = 0.214$ m/s; (B) $V = 0.432$ m/s; (C) $V = 0.486$ m/s; (D) $V = 0.540$ m/s. This figure is available in colour online at www.apjChemEng.com.

appeared to hinder the spreading of the coating at the same coating speed, resulting in a narrower stripe. The effect of solution viscosity was no longer significant when the viscosity exceeded 24 mPa s. On the other hand, the coating flow from a rectangular nozzle was more stable, and a much higher coating speed could be reached for low viscosity solutions, as observed in Fig. 8(b). However, this flow geometry was not suitable for high viscosity solutions. The stable coating range was found to be relatively narrow, and

DOI: 10.1002/apj

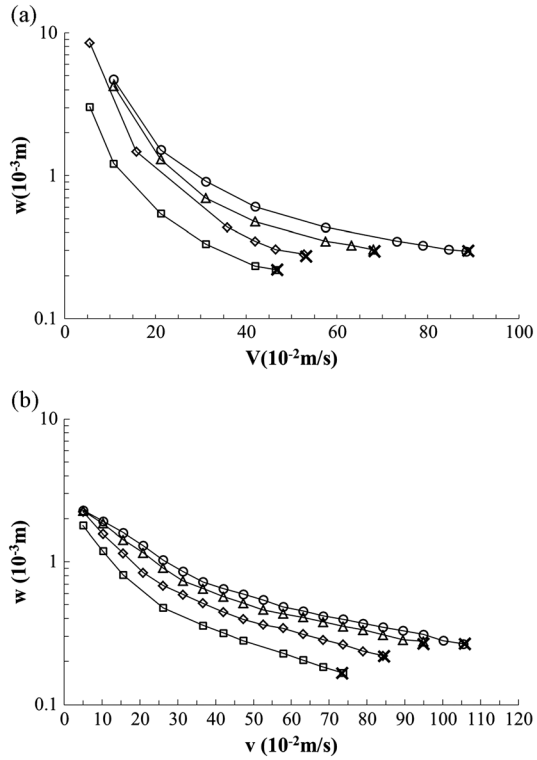

Figure 7. The effects of flow rate on the coating width variations $S = 1.0 \times 10^{-3}$ m, $H = 1.0 \times 10^{-3}$ m, $L = 2.0 \times 10^{-3}$ m, $W = 1.0 \times 10^{-3}$ m. $\mu = 6.5$ mPa s, ×: upper speed limit for coating; $\sigma = 42.5$ mN/m; □: $Q = 2.4 \times 10^{-6}$ kg/s; ◊: $Q = 4.67 \times 10^{-6}$ kg/s; △: $Q = 7.48 \times 10^{-6}$ kg/s; ○: $Q = 9.3 \times 10^{-6}$ kg/s; (a) slot die; (b) rectangular nozzle.

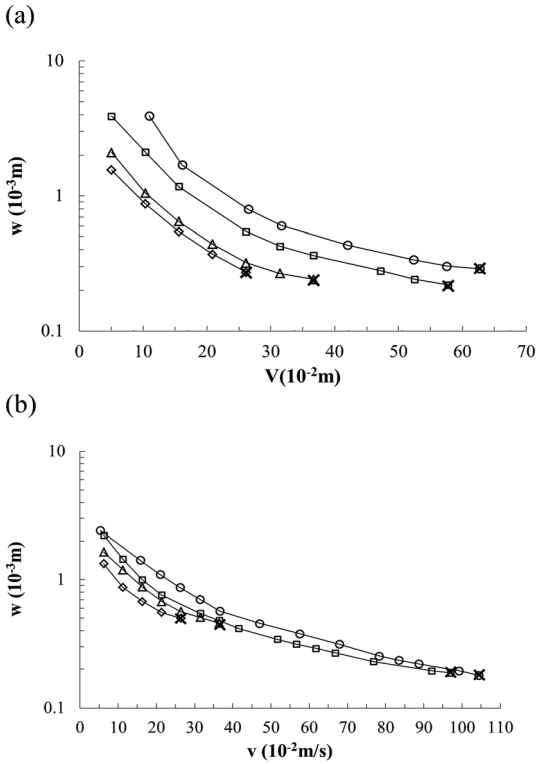

Figure 8. The effects of viscosity on the coating width variations $Q = 4.67 \times 10^{-6}$ kg/s; $S = 1.0 \times 10^{-3}$ m, $H = 1.0 \times 10^{-3}$ m, $L = 2.0 \times 10^{-3}$ m, $W = 1.0 \times 10^{-3}$ m. ×: upper speed limit for coating; ○: $\mu = 6.5$ mPa s, $\sigma = 21.5$ mN/m; □: $\mu = 10.0$ mPa s, $\sigma = 22.0$ mN/m; △: $\mu = 24.0$ mPa s, $\sigma = 21.1$ mN/m; ◊: $\mu = 45$ mPa s, $\sigma = 20.2$ mN/m; (a) slot die; (b) rectangular nozzle.

the coating bead was observed to vibrate vigorously before breakage. This flow instability phenomenon was not seen for low viscosity solutions.

The effect of the coating gap, H, on the coating stripe for the two flow geometries was next examined. As indicated in both Fig. 9(a) and (b), a larger coating gap seemed to destabilize the coating bead, causing the breakage of the coated stripe at a lower coating speed. At the same coating gap, the coating bead emanating from the rectangular nozzle was more stable for the low viscosity solution.

A dimensional analysis was used to estimate the relative effects of various operating variables and physical properties of the solution on the spreading of coated stripe. As noted earlier, the coated stripe would break when the coating width was reduced to approximately 20–30% of the slot channel width. To achieve a higher coating speed, it was essential to maintain the coated stripe as wide as possible. In the data analysis, all relevant parameters were divided into two groups: one of which favored the spreading of the stripe, whereas the other opposed the spreading. The favoring group was predominantly controlled by the coating solution flow rate; whereas the opposing group consisted of viscosity, surface tension, coating speed, and contact angle. The effects of these parameters are summarized into the following force terms:

(1) Viscous force: $\mu V/H$
(2) Inertial force in the slot channel: ρu^2
(3) Gravitational force: $\rho g h$
(4) Surface tension: σ/r, where $r \equiv w/(2\sin\theta_s)$

The relative importance of these forces on the flow behavior of the coated stripes was compared in terms of various dimensionless groups. The coating flow was moving vertically downward to deposit on a moving substrate, therefore gravity had to be taken into consideration. Two dimensionless groups, that is, capillary number Ca that represents the ratio of viscous force to surface tension and Reynolds number Re that represents the ratio of inertial force to viscous force, are usually used to present the results of coating flows.[8–13] Ca varied between 0.2 and 2, whereas Re varied between 0.01 and 10 in the present study. Several attempts were made; it was not possible to find a good correlation with a single dimensionless group.

DOI: 10.1002/apj

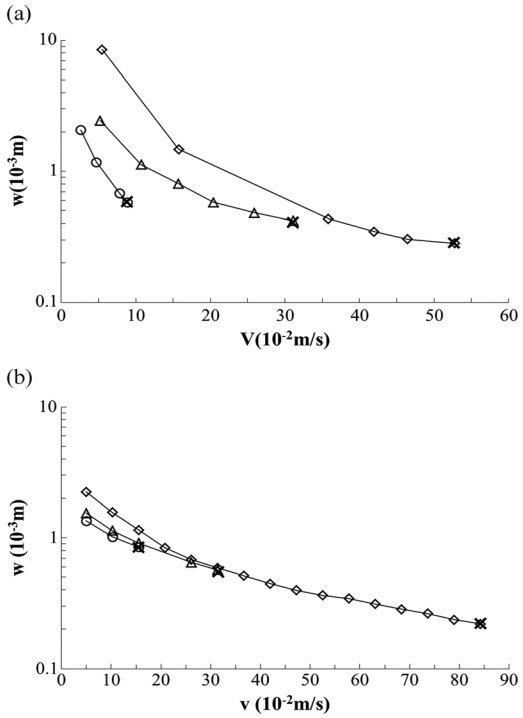

Figure 9. The effects of coating gap on the coating width variations $S = 1.0 \times 10^{-3}$ m, $L = 2.0 \times 10^{-3}$ m, $W = 1.0 \times 10^{-3}$ m, $\mu = 6.5$ mPa s, $\sigma = 42.5$ mN/m, ×: upper speed limit for coating; ◇: $H = 1.0 \times 10^{-4}$ m; △: $H = 3.0 \times 10^{-4}$ m; ○: $H = 5.0 \times 10^{-4}$ m; (a) slot die; (b) rectangular nozzle.

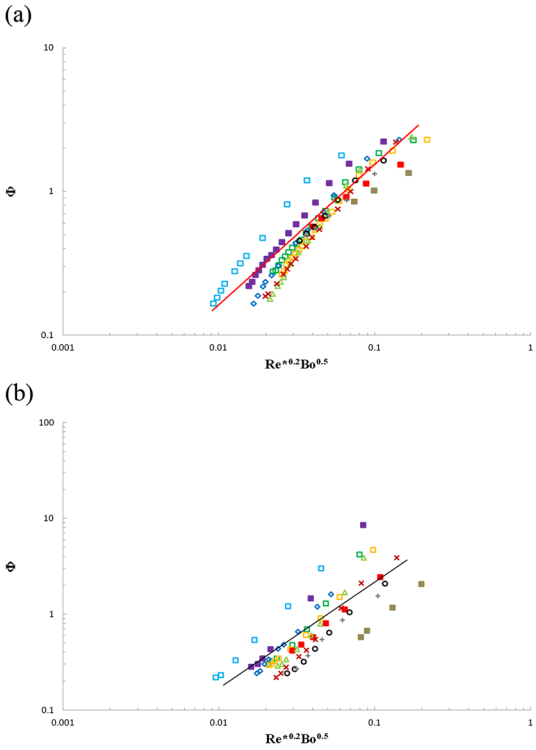

Figure 10. A universal correlation that involves the Reynolds number and the Bond number. The physical properties of the solutions are listed in Table 2. ($Q_1 = 2.4 \times 10^{-6}$ kg/s, $Q_2 = 4.67 \times 10^{-6}$ kg/s, $Q_3 = 7.48 \times 10^{-6}$ kg/s, $Q_4 = 9.3 \times 10^{-6}$ kg/s, $H_2 = 3.0 \times 10^{-4}$ m, $H_3 = 5.0 \times 10^{-4}$ m) □: number 1; : number 2; △: number 3; ×: number 4; ○: number 5; +: number 6; (a) slot die; (b) rectangular nozzle. This figure is available in colour online at www.apjChemEng.com.

A universal correlation was developed finally through a stepwise regression procedure to predict the variations of coating width with these forces. The dimensionless coating width ($\Phi = w/W$) was found to depend on two dimensionless groups: *Reynolds* and *Bond* numbers defined as

$$\mathrm{Re}^* \equiv \frac{pu^2}{\mu V/h} \tag{11}$$

$$Bo \equiv \frac{\rho g h}{\sigma/r} \tag{12}$$

The correlations of Φ with Re* and *Bo* for all experimentally obtained coating stripes with the slot die and rectangular nozzle are presented in Fig. 10(a) and (b), respectively. The least squares fitted correlation equations were found to be

$$\Phi = 26.0 \times \mathrm{Re}^{*0.2} Bo^{0.5} \quad \text{(13a) slot die}$$

with $R^2 = 0.665$

$$\text{and } \Phi = 14.20 \times \mathrm{Re}^{*0.2} Bo^{0.5} \quad \text{(13b) rectangular nozzle}$$

with $R^2 = 0.867$

The data in Fig. 10 appeared to be somewhat scattered. This could be due to the difficulty in measuring accurately the coating width. However, the previous correlations could at least serve as qualitative indicators on how each of these parameters would influence the coating width. For example, the equations indicated that the dependence of coating width on *Bo* was much stronger than on Re*, or the gravitational force was more dominant than the inertial force in determining the coating width for a coating solution of fixed viscosity and surface tension. Experimentally, it was found that the coated stripe Φ broke at around 0.2 and 0.3. Setting this value of Φ in Eqs. (13a) and (13b) would enable the prediction of the maximum coating speed by using the respective geometry.

The mechanism for the break-up of the narrow coated stripe produced using the slot die coating was illustrated by a sequence of photos of the coating bead shown in Fig. 11. For stable stripe coating, the coating bead was bound by the upstream and the downstream menisci and remained unchanged with increasing

DOI: 10.1002/apj

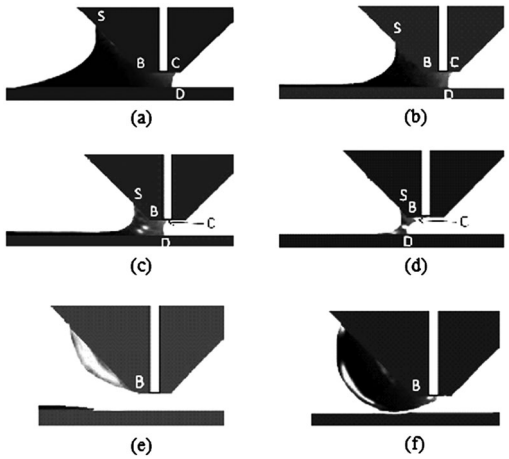

Figure 11. The photos showing how coating bead breaks. $\mu = 6$ mPa s, $\sigma = 43.1$ mN/m, $H = 2.0 \times 10^{-4}$ m, $W = 1.0 \times 10^{-3}$ m, $S = 1.0 \times 10^{-4}$ m, $Q = 6.0 \times 10^{-6}$ kg/s, $V = 0.25$ m/s, C: upstream contact line; S: downstream contact line; B: the die edge; D: the dynamic contact line of the bead.

coating speed (Fig. 11(a)). When the coating speed reached a critical value, the coating bead became unstable. The upstream meniscus moved first toward the slot exit (Fig. 11(b)); followed by the movement of the downstream meniscus toward the die lip (Fig. 11(c)). Finally, the coating bead broke and the coating solution was carried away by the moving web (Fig. 11(d)). Because the coating solution continued to emanate from the slot exit during the coating process after the breakage of the coating bead, the solution, instead of falling onto the moving web, would cling and climb on the wetted die lip (Fig. 11(e)). The hump on the die lip wall would grow, as shown in Fig. 11(f), until it became too heavy and fell onto the moving web. The coating process would then restart from the formation of a stable coating bead, similar to that shown in Fig. 11(a) and the periodic motion would repeat again. This break-up phenomenon was quite different from previous observations in the wide channel slot die coating where the high-speed defect was ribbing. The break-up velocity for the narrow stripe coating was also much higher than the conventional slot die coating.

Variations of the coating widths for stripes were further examined with numerical simulations by using a commercial software FLOW-3D. The predicted coating widths as a function of coating speed for three different solution flow rates that were compared with experimental results, as shown in Fig. 12. In the simulation, the upper coating speed limit was set at around 0.2–0.3 m/s; significant computing time is required to reach a convergent solution at higher coating speeds. It was found that a convergent solution could not be achieved if the spreading of the coated stripe was too wide. As seen in Fig. 12, the agreement was better for the narrower channel width, with a maximum difference between predictions and experimental results of around 15%. Hence, in the absence of experiments, one could confidently use the FLOW-3D package to predict, at least qualitatively, the coating width and flow field of narrow stripe coating provided the coating width contraction is not significant.

Figure 13 compares the numerical simulations obtained on a 3D narrow stripe coating flow with a 2D coating bead at the same flow rate per slot channel width q_s and different coating speeds. Figure 13(a-1), (b-1), and (c-1) show the three top views of the coated stripes obtained on the 3D simulation at increasing coating speed. At low speed, $V = 0.17$ m/s (Fig. 13(a-1)), the coating solution expanded laterally after emanating from the slot die, and the flow rate per unit coating width q_c was less than the flow rate per slot channel width q_s. At intermediate speed, $V = 0.24$ m/s and $q_c = q_s$, (Fig. 13(b-1)), no evidence of lateral expansion was observed. When the coating speed was further increased to $V = 0.35$ m/s, Fig. 13(c-1) shows that the resultant stripe width became narrower than the channel width or $q_c > q_s$, indicating a contraction of the coating solution.

The remaining figures in Fig. 13 compare the predicted coating bead shapes based on 3D and 2D simulations at three coating speeds. In the 2D simulation, q_s was assumed to be always the same as q_c. At low speed, $V = 0.17$ m/s, the coating bead simulated from the 3D solution (Fig. 13(a-2)) was seen to be smaller than the one predicted by the 2D simulation, (Fig. 13(a-3)). In the 2D simulation, the upstream of the coating bead was closer to the rear end of the die lip corner, and dripping appeared to occur. By contrast, the coating bead predicted by the

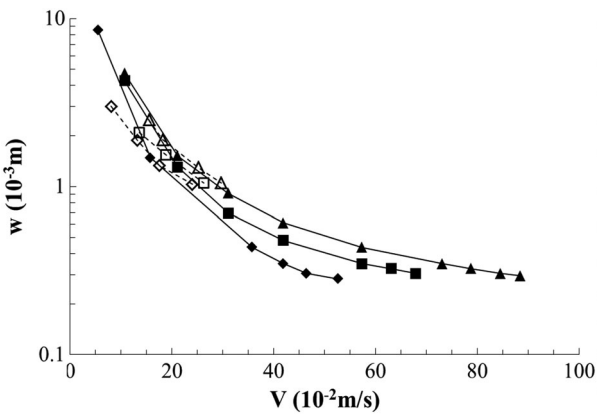

Figure 12. Comparison of the experimental findings with the theoretical predictions. Solid symbols: experimental results; hollow symbols: theoretical prediction. $S = 1.0 \times 10^{-3}$ m, $H = 1.0 \times 10^{-3}$ m, $L = 2.0 \times 10^{-3}$ m, $W = 1.0 \times 10^{-3}$ m; $\mu = 6.5$ mPa s, $\sigma = 42.5$ mN/m; (◆), ( ): $Q = 4.67 \times 10^{-6}$ kg/s; (■), (□): $Q = 7.48 \times 10^{-6}$ kg/s, (▲), (Δ): $Q = 9.3 \times 10^{-6}$ kg/s.

DOI: 10.1002/apj

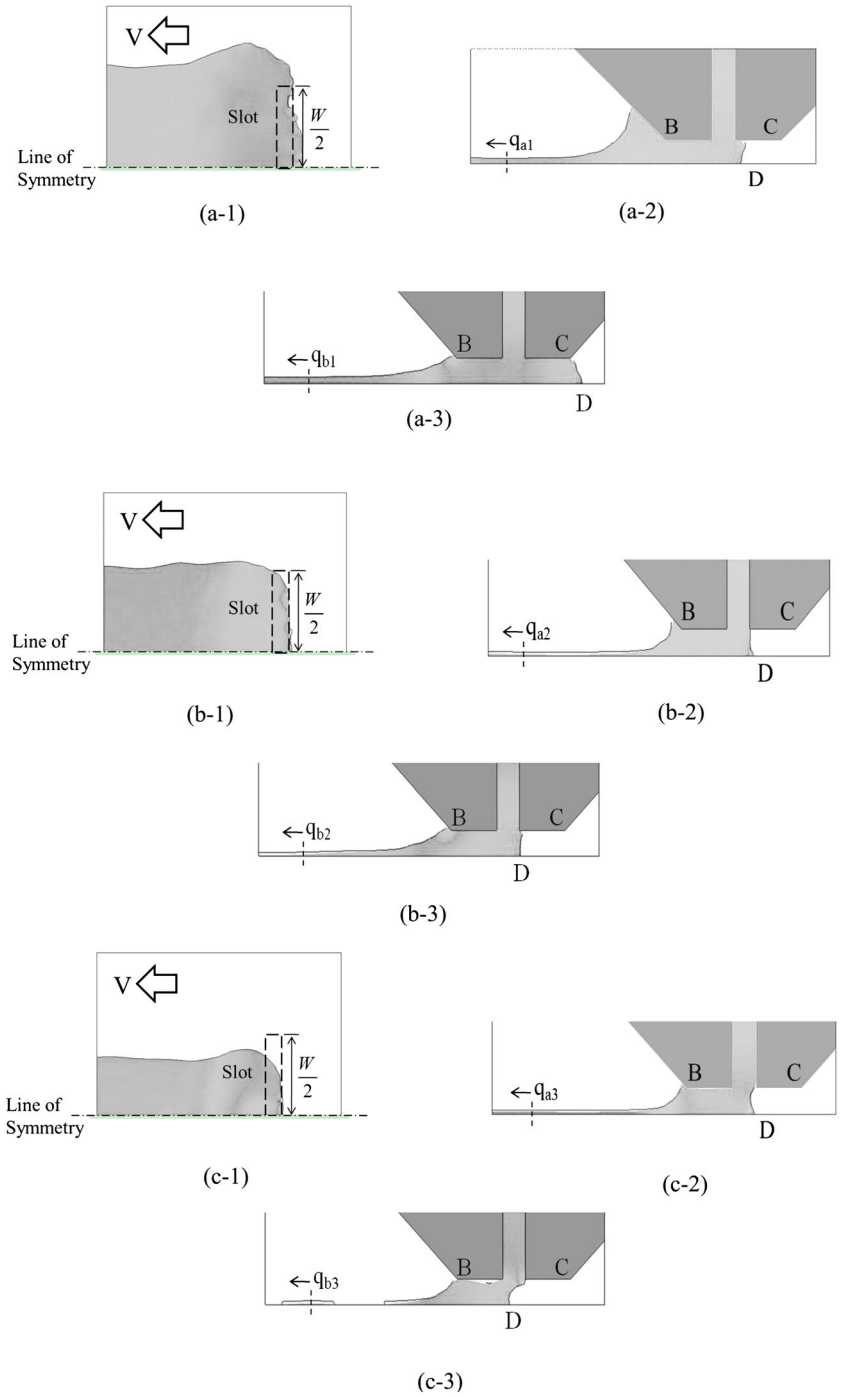

Figure 13. The difference between 3D and 2D coating simulations. $\mu = 6$ mPa s, $\sigma = 43.1$ mN/m, $H = 1.0 \times 10^{-4}$ m, $L = 2.0 \times 10^{-4}$ m, $Q = 4.67 \times 10^{-6}$ kg/s. B: the die edge; C: the downstream static contact line of the coating bead; D: the dynamic contact line of the coating bead; (a-1): the top view in 3D simulation, $V = 0.17$ m/s; (a-2): the side view in 3D simulation, $V = 0.17$ m/s; (a-3): the result of 2D simulation, $V = 0.17$ m/s; (b-1): the top view in 3D simulation, $V = 0.24$ m/s; (b-2): the side view in 3D simulation, $V = 0.24$ m/s; (b-3): the result of 2D simulation, $V = 0.24$ m/s; (c-1): the top view in 3D simulation, $V = 0.35$ m/s; (c-2): the side view in 3D simulation, $V = 0.35$ m/s; (c-3): the result of 2D simulation, $V = 0.35$m/s. This figure is available in colour online at www.apjChemEng.com.

3D simulation was smaller and more stable. The spreading of the narrow coated stripe at low coating speed appeared to stabilize the coating bead. At intermediate speed, $V = 0.24$ m/s, the simulated coating bead shapes from the 3D and 2D solutions were similar, as seen in Fig. 13(b-2) and (b-3), suggesting

DOI: 10.1002/apj

that the coating width predicted by the 3D simulation was very close to the slot channel width, or $q_s = q_c$. Hence, a simpler 2D simulation could be used to predict the shape of the coating bead at this condition. Lastly, the 3D prediction of coating width (Fig. 13(c-2)) was seen to be smaller than the channel width or $q_c > q_s$. Because it was assumed that $q_c = q_s$ in the 2D simulation, it would be expected that a lesser flow in the coating bead region, as indicated by the void region underneath the downstream die lip (Fig. 13(c-3)). Also, the upstream meniscus was highly distorted and the coating bead was unstable. The results shown in Fig. 13 clearly indicated that, because of the ability of the coating solution to spread or contract laterally, coated stripes obtained from the narrow strip coating was more stable than from a conventional slot coating machine.

CONCLUSIONS

The fluid mechanics of coating a narrow stripe with low viscosity Newtonian solutions was studied. Either a slot die fitted with a shim of specified width or a rectangular nozzle could be used to create a narrow stripe. As the flow channel width was systematically reduced, the coating defect at high coating speeds would switch from a commonly observed ribbing to a repeated *coat-and-break* pattern. The transition channel width was found to be between 2 and 4×10^{-4} m. Only the coat-and-break defect was observed for channel width of 1×10^{-4} m or less. This coating defect appeared at a coating speed much higher than that for the conventional onset of ribbing.

In the narrow stripe coating, the coating width was found to either expand or contract laterally after emanating from the slot die channel depending on the coating speed. The maximum coating speed occurred at a coating width of around 20–30% of the flow channel width.

The effects of physical properties and operating variables on the coating width were examined. The parameters were divided into two dimensionless groups: Reynolds and Bond numbers. The group involving flow rate was responsible for the spreading of coating width; whereas the other involving viscosity, surface tension and coating speed was responsible for the contraction of coating width. A universal correlation was obtained that could be used to estimate the coating width and the maximum coating speed.

The mechanism of narrow stripe break-up was investigated both experimentally and theoretically. A flow visualization technique was utilized to observe the fluid motion in the coating bead region above the maximum coating speed for stable coating. Both upstream and downstream menisci of the coating bead were seen to approach each other until breakage occurred. During this period, the coating solution emanating from the slot die exit continued to accumulate on the downstream die lip region afterwards until it became too heavy and fell off onto the moving substrate. The process of the formation and break-up of narrow stripe was periodical.

The 3D simulation of the narrow stripe coating flow was able to predict the lateral expansion and contraction of the coating solution emanating from the die. The predicted coating bead was more stable compared with that obtained from the conventional 2D slot die coating.

Acknowledgement

This research was supported by the National Science Council, Taiwan, under Grant No. NSC 99-2221-E-007-090-M73.

Notations:

Bo	: bond number, $\frac{\rho g h}{\sigma / r}$
Ca	: capillary number, $\frac{\mu V / H}{\sigma / r}$
g	: gravitational factor
H	: coating gap (m)
h	: average coating thickness, Q/(V w) (m)
k	: unit vector in gravitational direction
n	: outward unit normal vector
p	: pressure of the coating solution (pa)
P	: dimensionless atmospheric pressure
P_{atm}	: atmospheric pressure (pa)
Q	: total flow rate (m^3/s)
q	: volumetric flow rate per unit coating width (m^2/s)
r	: nominal radius of the stripe ($r \equiv w/(2\sin\theta_s)$) (m)
S	: slot gap(m)
St	:S tokes number, $\rho g H^2/\mu V$
T	: stress tensor (N/m^2)
Re	Reynolds number,ρq/μ
Re^*	: a modified Reynolds number, $\frac{\rho\left(\frac{Q}{S \cdot w}\right)^2}{\mu\frac{V}{H}}$
r	: nominal radius of the stripe, $w/(2\sin\theta_s)$ (m)
u	: average fluid speed in the slot (m/s)
V	: web speed (m/s)
v	: velocity vector (m/s)
W	: width of the slot channel (m)
w	: width of the coated stripe (m)

Greek letters:

Φ	: dimensionless width of the coated stripe ($\Phi \equiv w/W$)
ρ	: fluid density (kg/m^3)
μ	: viscosity (Pa s)
σ	: surface tension (J/m^2)
θ_s	: static contact angle on the liquid side (°)

DOI: 10.1002/apj

REFERENCES

[1] P. Haaland, J. Mackibben, M. Parodi, *Solid State Technol*, **1995** ; *38*, 83–89.
[2] S. Kokubo, T. Yoshikawa, N. Osano. *JP. Patent*, **2003**; 344–642.
[3] Y.C. Lin, Y.Y. Lin, D.S.H. Wong, T.J. Liu, S.H. Wen, K.T. Huang. *J. Appl. Polym. Sci.*, **2011**; *120*, 1555–1565.
[4] S.H. Wen, T.J. Liu. *Polym. Eng. Sci.*, **1995**; *35*, 759–767.
[5] E. Beguin, *U.S. Patent*, **1954**; *2* 681 294.
[6] K.J. Ruschak. *Chem. Eng. Sci.*, **1976**; *31*, 1057–1060.
[7] B.G. Higgins, L.E. Scriven. *Chem. Eng. Sci.*, **1980**; *35*, 673–682.
[8] K.Y. Lee, L.D. Liu, T.J. Liu. *Chem. Eng. Sci.*, **1992**; *47*, 1703–1713.
[9] M.S. Carvalho, H.S. Kheshgi. *AIChE J.*, **2000**; *46*, 1907–1917.
[10] Y.R. Chang, H.M. Chang, C.F. Lin, T.J. Liu. *J. Colloid & Inter. Sci.*, **2007**; *308*, 222–230.
[11] Y.R. Chang, C.F. Lin, T.J. Liu. *Polym. Eng. Sci.*, **2009**; *49*, 1158–1167.
[12] H.M. Chang, Y.R. Chang, C.F. Lin, T.J. Liu. *Polym. Eng. Sci.*, **2007**; *47*, 1927–1936.
[13] H.M. Chang, C.C. Lee, T.J. Liu. *Int. Polym. Proc.*, **2009**; *24*, 157–165.
[14] T. Dobroth, L. Erwin. *Polym. Eng. Sci.*, **1986**; *26*, 462–467.
[15] H.E. Huppert. *J. Fluid Mech.*, **1982**; *121*, 43–58.
[16] S. Vafaei, M.Z. Podowski. *Interface Sci.*, **2005**; *113*, 133–146.
[17] C.L. Bower, E.A. Simister, E. Bonnist, K. Paul, N. Pightling, T.D. Blake. *AIChE J.*, **2007**; *53*, 1644–1657.
[18] T.J. Liu, Y.W. Yu. *U.S. Patent*, **2000**; *6*, 159–544.
[19] T.J. Liu, Y.W. Yu. *U.S. Patent*, **2002**; *6*, 423–140.
[20] C.W. Hirt, J.E. Richardson, K.S. Chen, In Proceedings of 50th Annual Conference of the Society for Imaging and Science Technology, Boston MA, **1997;** 458–463.
[21] C.W. Hirt, B.D. Nicols, J. Comput. *Phys.*, **1981**; *39*, 201–225.
[22] C.F. Lin. Fundamental Study of Narrow Stripe Coating. , Ph. D. Thesis, Taiwan, NTHU, **2009**; pp.1–147.

DOI: 10.1002/apj